Undesirable Haemodynamics in Aneurysms

Gregory J. SHEARD,[1,3,†] **Roger G. EVANS,**[1,2] **Kate M. DENTON**[1,2] **and Kerry HOURIGAN**[1,3]

[1] *Monash University Biomedical Engineering Technology Alliance (MuBeta), Monash University, VIC 3800, Australia.*
[2] *Department of Physiology, Faculty of Medicine, Nursing and Health Sciences, Monash University, VIC 3800, Australia.*
[3] *Fluids Laboratory for Aeronautical and Industrial Research (FLAIR), Department of Mechanical Engineering, Monash University, VIC 3800, Australia.*
[†] *Corresponding author:* Greg.Sheard@eng.monash.edu.au

Abstract. A computational fluid dynamics study is employed to investigate the flow within an idealized fusiform aneurysm. The model includes sections of the arteries upstream and downstream of the aneurysm, which is modeled as an elliptical bulge of a shape consistent with both previous experimental studies, and accepted values for aneurysms located on the human abdominal aorta. Flow is assumed axisymmetric and Newtonian, allowing efficient computation in cylindrical coordinates. Results are reported for both a steady-state inflow, as well as time-varying inputs with frequencies selected to represent heart rates ranging from rest to strenuous exercise. The effects of these parameters on the dynamics of the flow within the aneurysm are reported, as is variation in the resistance to flow when compared with an undeformed artery of the same length.
The rate at which fluid is flushed from an aneurysm is found to be strongly dependent on the frequency of the pulsatile flow, but independent of geometrical features such as the radius of curvature at the junction between the artery and the aneurysmal bulge. Wall shear stress and pressure drop across the aneurysm are found to be sensitive to these geometrical alterations, although in the case of the pressure drop the changes are insignificant as the resistance to flow is predicted to be lower in the aneurysm than in an undamaged artery of the same length.

Key words: Aneurysm, blood flow, fusiform, haemodynamics, particle tracking, direct numerical simulation, spectral element method.

1. Introduction

Aneurysms are localized dilations of arteries, and typically develop in the aorta, carotid artery, and cerebral vessels. They arise from a weakness in the vessel wall, usually in regions of high wall shear stress (hereafter WSS). High-shear regions are usually encountered near a branch point or other regions of non-uniformity [7]. The development of aneurysms follows a vicious cycle whereby increased peak wall stress within the developing aneurysm weakens the vessel wall, so causing enlargement of the aneurysm and further increases in peak wall stress. Simultaneously, shear stress appears to increase in proportion to the growth of the aneurysm, and is thought to drive the molecular mechanisms underlying aneurysm progression [7, 8]. Aneurysms of the abdominal aorta typically widen at a rate of approximately 4 mm per year [11]. Rupture of aneurysms is believed to occur when the mechanical stress acting on the wall exceeds the strength of the wall tissue. Degeneration of the vascular wall, and

so reduced wall strength, is evidenced by the observation that ruptured aneurysms contain fewer smooth muscle cells and more irregular layers of collagen IV than the walls of unruptured aneurysms [6]. Endothelial damage and inflammatory cell invasion of the vascular wall are also hallmarks of ruptured aneurysms [6]. Recent interest has surrounded the wall stress distribution within aneurysms with a view to development of a predictive model to quantify their growth and eventual rupture. This would be a major development in the clinical management of aneurysms, but this field is presently in its infancy. Blood flow dynamics likely also make a major contribution to the pathogenesis, progression, and possible rupture of aneurysms. For example, recent reports support the hypothesis that WSS contributes to the genesis of aneurysms [7]. The presence of foci of high WSS is likely a major factor leading to aneurysm formation in previously healthy arteries. Animal models of aneurysm formation suggest that increased WSS can lead to degenerative changes in the vascular endothelium that progress to the underlying vascular smooth muscle. The present computations will demonstrate that aneurysms with a gradual contraction at the distal end expose healthy artery wall tissue to adverse WSS conditions, as the peak WSS location occurs further downstream in those cases.

Another issue that must be considered is the appearance of areas of stagnation of blood flow, which occurs particularly in large aneurysms such as those that develop in the abdominal aorta [9]. Stagnation of blood flow results in aggregation of red blood cells and the accumulation and adhesion of platelets and leucocytes along the intimal surface of the vasculature. This is likely exacerbated by evolving endothelial injury. In turn, these factors can lead to the development of intra-aneurysmal thromboses, and subsequent infarction of downstream vascular beds if a thrombus detaches, or if the thrombus remains in situ, inflammatory changes in the aneurysm wall that will further weaken it and increase the risk of rupture. There is also evidence that abdominal aortic aneurysms can induce a state of systemic hypercoagulopathy, the severity of which is proportional to the aspect ratio of the aneurysms [9].

The structure and dynamics of flow within aneurysms has been measured in numerous *in vitro* and *in vivo* studies. In a rabbit model, Doppler ultrasound was used [19] to obtain the velocity field within aneurysms of various sizes. The Reynolds number and Womersley number of this model mimicked human cerebral arteries. Tagged image velocimetry has been applied to study the flow in a replica intracranial aneurysm [4]. The study produced velocity vectors, vorticity and shear strains throughout the model at 9 ms intervals. Digital particle image velocimetry has been used to calculate wall shear stress and fluid shear rate in fusiform aneurysm models [8]. The measured flow fields comprised a fast flow through the core of the aneurysm, following the vessel axis, and a slowly rotating ring of fluid between the core and the aneurysm wall.

Studies of wall stresses in abdominal aortic aneurysms show these to be greatly elevated within the aneurysm [12], with peak wall stress located in the vicinity of the posterior wall. Some attempts have been made to use computational fluid dynamics to determine a predictive model of aortic aneurysm rupture [11], based on realistic aneurysm morphology derived from clinical imaging. Steinman *et al.*[17, 18] recently described a case report of such an analysis.

Computational fluid dynamics presents an increasingly valuable tool for the study and risk assessment of aneurysmal blood flow. This literature review has identi-

fied that regions of high wall shear stress act to weaken vessel walls and therefore promote the growth of an aneurysm, and that stagnant regions resulting from incomplete fluid replacement within aneurysms can lead to clot formation and subsequent infarction of a downstream vascular bed. There is speculation that blood flow within aneurysms is highly dependent on the precise geometry of the aneurysm and the nature of the input haemodynamics [17, 18], and thus idealized models are thought to provide a poor approximation to the flow in anatomically realistic vessels [10]. The primary hypothesis of this study is: The wall shear stress and rate of fluid replacement within an aneurysm are sensitive to geometry modifications consistent with an idealization of a realistic aneurysm geometry.

This study will investigate the flow in a model fusiform aneurysm with dimensions consistent with earlier experimental studies (e.g., [2]). The computational domain consists of straight circular arteries, which are joined to the proximal (upstream) and distal (downstream) ends of an elliptical bulge with length-to-width ratio 1.76 and length $4D$. This model is shown schematically in figure 1. This idealized geometry is modified to better represent realistic aneurysms by systematically smoothing the junction points between the healthy arterial segments and the aneurysm. The effect of this modification on the flow properties is the focus of this study.

2. Methodology

Numerical simulations are performed using a high-order spectral-element technique formulated in cylindrical coordinates [15, 16]. For computational convenience, flow quantities are normalized: i.e., velocity by mean inlet velocity U and length by artery calibre D. Combining these with the kinematic viscosity of blood, ν, a Reynolds number is defined

$$Re = \frac{UD}{\nu}.$$

This study will investigate a physiologically significant range of Reynolds numbers $100 \leq Re \leq 2000$.

Due to the azimuthal symmetry of the geometry, the flow is computed on the meridional half-plane. An example of the meshes used is shown in figure 2. At the inlet, a parabolic velocity profile is employed for steady and unsteady simulations. The aneurysm and vessel walls are treated as rigid, impermeable boundaries where a zero-velocity no-slip condition is prescribed. At the outlet, a reference pressure is prescribed, and a zero normal gradient of velocity is naturally enforced as a result of the numerical formulation [5].

Numerical flow visualization is employed by seeding the flow with passive tracer particles. The trajectory of these particles is computed using an approximately 4^{th}-order Runge–Kutta hybrid parametric/physical space integration scheme (e.g., see [1]). The particle concentration is recorded at each interpolation point, subject to a local two-dimensional Gaussian filter with a standard deviation chosen to scale with local mesh density. Plotting contours of particle concentration achieves similar results to experimental dye visualization techniques [14, 13].

To examine the results in a physiological context, dimensional results are also presented, based on reference conditions for the human abdominal aorta [3]; i.e., calibre

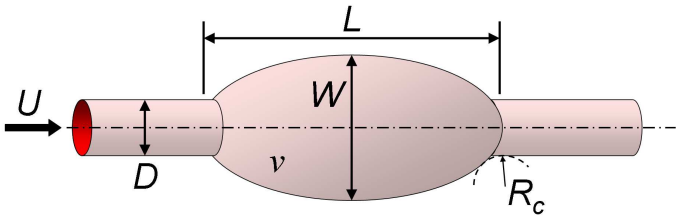

Figure 1. Schematic diagram showing the aneurysm model under investigation. In this study L/W is maintained at 1.76, and $L = 4D$. The proximal and distal artery segments are each $3D$ in length, and the radius of curvature (R_c) of the idealized junction between the artery and aneurysm is shown.

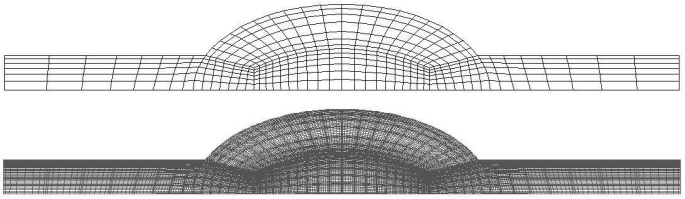

Figure 2. A mesh employed in this study. Top: Spectral elements are shown. Bottom: Interpolation points within elements are also shown. Due to symmetry, only the meridional half-plane is required to be discretized.

$D = 20$ mm, density $\rho = 1060$ kg/m^3, kinematic viscosity $\nu = 2.547 \times 10^{-6}$ m^2/s. The heart rate frequency f is described by the non-dimensional Womersley number

$$\alpha = \frac{1}{2} D \sqrt{2\pi f/\nu}.$$

A range $12 \leq \alpha \leq 25.2$ is investigated, corresponding to heart rates between 35 and 154 beats per minute. This study employed a sinusoidal function of velocity, the fluctuating component of which had an amplitude of $U/2$.

3. Validation

To verify the accuracy of the simulations, a grid-independence study was performed, and further comparisons were made with limited available experimental data on a similar aneurysm model. A test case was simulated over a range of element polynomial degrees at $Re = 2000$ with a steady-state inlet flow. An L_2 norm of the velocity field was recorded when the simulations reached a steady state, and a percentage error was taken from the difference between each case and the highest-resolution case. The results are plotted in figure 3, which shows a rapid spatial convergence. From these results, it was decided to perform the computations in this study at the efficient element polynomial degree $N = 5$.

An experimental dye-visualization study [2] has presented images of flow in a model abdominal aortic aneurysm consistent with the present model. Simulated-particle computations were performed under matching flow conditions, and visualizations of the flow at a corresponding point in the pulse cycle is shown in figure 4. The

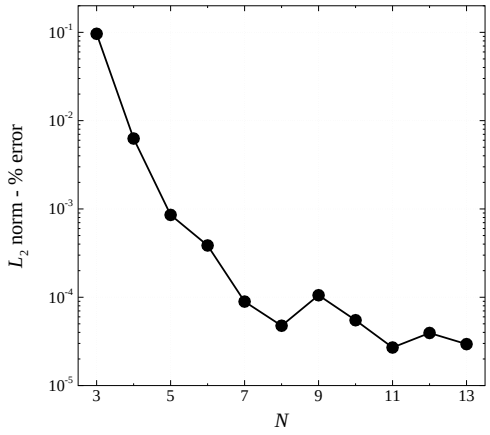

Figure 3. Percentage error in L_2 norm ($=\int_{\mathcal{V}} |\mathbf{u}|\, \mathrm{d}\mathcal{V}$, where $\mathcal{V}$ is the computational domain volume) of velocity plotted against element polynomial degree N. A steady inflow at $Re = 2000$ was employed as a test case. Rapid spatial convergence is demonstrated.

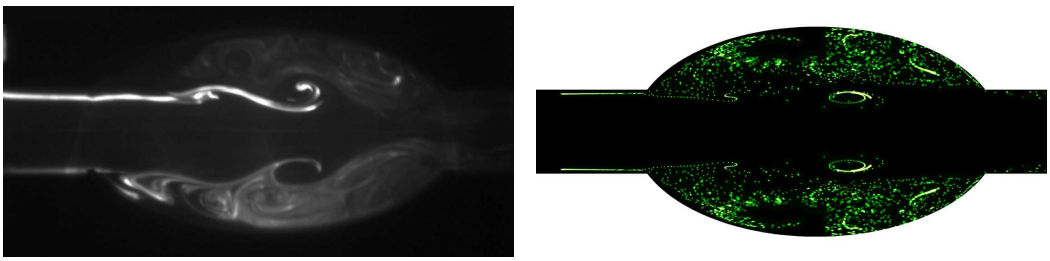

Figure 4. Comparison between (left) experimental dye visualization and (right) simulations at $Re = 2000$ and $\alpha = 22.5$. Flow is from left to right in each frame. Lighter shades indicate regions of high particle/dye concentration.

comparison shows that dynamical flow features are correctly reproduced. These include the large vortex ring moving along the axis just downstream of the centre of the aneurysm, the entrainment of particles in the recirculating fluid within the bulge, and the smaller vortical perturbation to the particle thread half way between the large vortex ring and the proximal end of the aneurysm.

4. Results: Steady Inflow

The steady-state flow in the model aneurysm was computed at a range of Reynolds numbers, with pressure drop and maximum WSS recorded for each case. To ascertain the sensitivity of flow to changes relating to the level of idealization in the geometry, the model was modified to incorporate rounded junctions between the artery and the proximal and distal ends of the aneurysm bulge. The radius of curvature of this smoothing was systematically varied over $0 \leq R_c/D \leq 3$, with zero corresponding to the sharp corners visible in figure 2. For these computations a constant Reynolds number $Re = 2000$ was employed, and again the pressure drop and maximum WSS were recorded.

With variation in Reynolds number, the location of maximum wall shear rate consistently occurred at the distal intersection between the artery and aneurysm bulge, due to the rapid deflection of attached flow from the contraction into the straight pipe section. Poiseuille's law dictates that the wall shear rate in a straight pipe should equal $8U/D$, which indeed was found in the straight pipe sections. However, at the distal corner, local values some 5 times higher than this value were obtained, varying from $42.8U/D$ at $Re = 100$ down to $35.6U/D$ at $Re = 100$. At other locations around the aneurysm wall, shear rates much lower than $8U/D$ were recorded, in support of earlier observations that abnormal levels of shear are associated with aneurysmal blood flow. Converting to a dimensional WSS, the values increased with mean inflow velocity from 4.68×10^{-2} Nm^{-2} with $U = 1.27$ cm/s to 15.6 Nm^{-2} with $U = 25.5$ cm/s, consistently in the order of 5 times greater than the values expected in a uniform artery.

The aneurysm presents the flow with an expansion followed by a contraction, and in this region mean flow velocities, wall velocity gradients, and hence friction, are lower. It was therefore unsurprising that the pressure drops computed across an aneurysm were lower than expected from a healthy artery of the same length. Consistently, the actual pressure drop was found to be between 75% and 80% of the corresponding drop expected from Poiseuille's law. For velocities ranging over $1.27 \leq U \leq 25.5$ cm/s, this corresponds to pressure drops ranging from $0.0032 \leq \Delta p \leq 0.062$ mmHg.

With variation in fillet radius of curvature, some interesting effects were observed. The smoothly varying wall curvature meant that the location of maximum WSS was no longer confined to the sharp corner at the distal end of the bulge. With increasing radius of curvature, the location of maximum WSS migrated *downstream* by $0.87D$ as R_c/D increased from 0 to 3. This was coupled with a large decrease in the maximum wall shear rate from $35.6U/D$ to $15.8D$ (here less than twice the value for a straight pipe from Poiseuille's law) over this range. Dimensionally, WSS decreased from 15.6 to 6.93 Nm^{-2} as R_c increased from 0 to 6 cm. These trends are plotted in figure 5.

Plots of the shear rate in the vicinity of the distal end of the aneurysm models are shown in figure 6. Regions of high shear rate at a wall correspond to regions of high WSS. These images show that elevated levels of WSS extend downstream into the healthy distal artery, which may lead to further weakening of the artery wall, and a subsequent lengthening and widening of the aneurysm, as reported by Lasheras [8].

5. Results: Pulsatile Inflow

An interesting feature of pulsatile flows was the development of nearly-stagnant recirculation zones located on the proximal wall of the aneurysm. These zones were, for some Womersley numbers, bounded by a closed streamline throughout the entire pulse cycle. This meant that the fluid retained within those zones never washed out of the aneurysm. Simulations were conducted at $Re = 2000$ for $\alpha = 16.9$ and 22.5 for a periodic flow uniformly seeded with particles at the beginning of the computation. Over a number of periods, these particles were progressively washed out of the computational domain. However, as can be seen in figure 7, the case with $\alpha = 16.9$ exhibited a closed stagnant region on the proximal wall, which could indicate a propensity for the development of clots through the stagnation and coagulation of

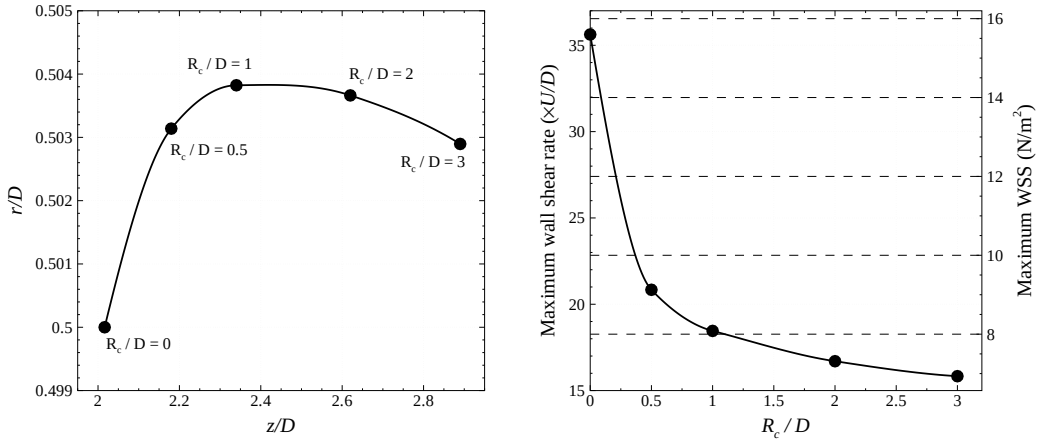

Figure 5. Left: Maximum wall shear rate and maximum dimensional WSS plotted against fillet radius of curvature. Right: Movement in the location of maximum shear stress. The origin of the z–r coordinate system is taken to be at the centre of the aneurysm.

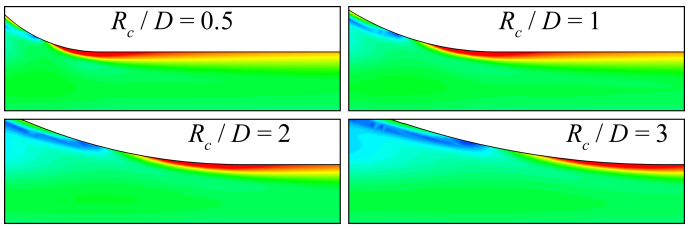

Figure 6. Contour plots of shear rate in the vicinity of the downstream end of the aneurysm wall for a number of wall curvatures. Blue and red contours show low and high shear rates, respectively. A steady inflow at $Re = 2000$ was applied in each case. Each frame is labeled with the radius of curvature for that simulation.

red blood cells.

To quantify the observations depicted in figure 7, the number of particles within the computational domain was recorded for a number of cases. Figure 8 show the rates at which particles exited the domain with variation in Womersley number (left) and fillet curvature (right). Two key conclusions can be drawn from these plots. Firstly, the frequency of the heartbeat has a significant effect on the time taken for fluid within the aneurysmal bulge to be convected out of the bulge, with the fastest removal, demonstrated by the steepest gradient, occurring with $\alpha = 20$, or 97 bpm based on the stated reference dimensional values. Secondly, the idealization of the aneurysm shape (i.e., the wall curvature at the proximal and distal ends of the aneurysm) has no noticeable effect on the rate of elimination of fluid from the aneurysm. Notice also that at lower frequencies, clearly visible plateaus in the number-of-particle trends are visible, corresponding to durations of each heartbeat where no aneurysmal fluid exits the domain.

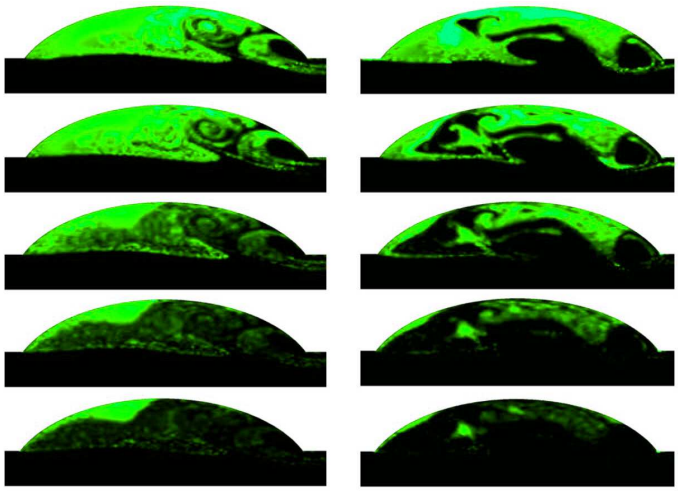

Figure 7. Particle concentration within an aneurysm over several periods. Time increases from top to bottom. Womersley numbers $\alpha = 16.9$ (left) and 22.5 (right) are compared, corresponding to heart rates of 70 and 123 beats per minute, respectively, if $D = 20$ mm and $\nu = 2.547 \times 10^{-6}$ m^2/s. Flow is left to right, and light shaded regions show concentration of tracer particles.

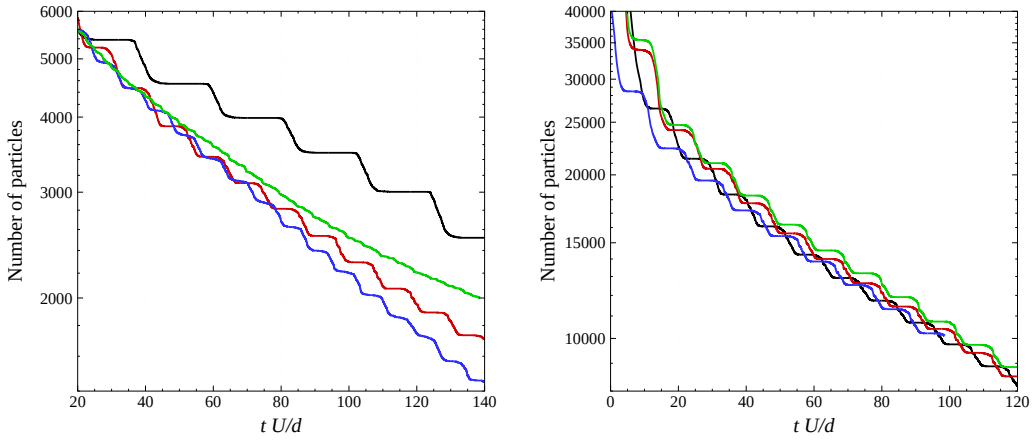

Figure 8. Number of particles in the computational domain plotted against non-dimensional time tU/D. A faster decrease corresponds to more rapid elimination of blood from the aneurysmal bulge, and pulsatile simulations were performed at $Re = 2000$. Left: Trends show Womersley numbers $\alpha = 12$ (black), 16.9 (red), 20 (blue), and 25.2 (green). Right: With a constant $\alpha = 16.9$, trends show $R_c/D = 0.5$ (black), 1 (red), 2 (blue), and 3 (green).

6. Conclusions

A computational investigation has been carried out to explore the fluid dynamics associated with aneurysmal blood flow. An axisymmetric model aneurysm was used, comprising an elliptical bulge with aspect ratio 1.76 and a length of four times the artery calibre. The original hypothesis of this study was partially confirmed, as wall shear stress was found to be sensitive to idealization of the geometry, though the rate of fluid replacement was not. Simulations with a steady inflow at a range of Reynolds numbers found that the maximum WSS was consistently 5 times higher than for uniform flow in a straight artery, and this occurred at the junction between the aneurysm and the distal artery. When the unnaturally sharp junctions were replaced by smooth rounded corners, a rapid decrease in the maximum wall shear stress with increasing curvature radius was found. In addition to this, the location of maximum wall shear stress propagated further downstream, moving towards the undamaged distal artery. This may be a significant factor in the feedback mechanism promoting aneurysm growth.

The aneurysm models tested were found to exhibit a low resistance to flow. Pressure drops across the aneurysms were between 20% to 25% lower than the pressure drop across an undeformed artery of the same length. With rounded fillets at the entrance and exit of the aneurysm, the pressure drop was reduced by as much as 40% below the undeformed artery value. It can be confirmed that flow quantities critical to the integrity of the vessel walls, such as wall shear stress, are sensitive to changes in the shape of an aneurysm. This is not the case for the rate of fluid replacement within the aneurysmal bulge. These computations reveal that under pulsatile flow conditions, variation in heartbeat frequency can dramatically alter the size and persistence of stagnant fluid regions within the aneurysm, and therefore impact the likelihood of clot formation, whereas alteration of the geometry by varying R_c had no impact on the rate at which fluid is replaced in the aneurysm.

Acknowledgements

G.J.S. received salary as an Australian Postdoctoral Fellow under ARC Discovery Grant DP0555987 from the Australian Research Council. This grant also supported the other authors. The computational resources of the Australian Partnership for Advanced Computing were utilized to complete this study, thanks to a time allocation under the Merit Allocation Scheme.

References

[1] G. Coppola, S. J. Sherwin, and J. Peiró. Non-linear particle tracking for high-order elements. *J. Comp. Phys.*, 172:356–386, 2001.

[2] R. Cowling and J. Soria. Flow visualisation through model abdominal aortic aneurysm. In *Proceedings of the Fourth Australian Conference on Laser Diagnostics in Fluid Mechanics and Combustion*, pages 33–36, The University of Adelaide, South Australia, Australia, 2005.

[3] A. C. Guyton and J. E. Hall. *Textbook of Medical Physiology, 11th edition.* W.B. Saunders, Philadelphia, 2006.

[4] H. Isoda, S. Inagawa, H. Takeda, S. Isogai, Y. Takehara, and H. Sakahara. Preliminary study of tagged MR image velocimetry in a replica of an intracranial aneurysm. *AJNR Am. J. Neuroradiol.*, 24(4):604–607, 2003.

[5] G. E. Karniadakis and S. J. Sherwin. *Spectral/*hp *Element Methods for Computational Fluid Dynamics*. Oxford University Press, 2005.

[6] K. Kataoka, M. Taneda, T. Asai, A. Kinoshita, M. Ito, and R. Kuroda. Structural fragility and inflammatory response of ruptured cerebral aneurysms. A comparative study between ruptured and unruptured cerebral aneurysms. *Stroke*, 30(7):1396–1401, 1999.

[7] S. Kondo, N. Hashimoto, H. Kikuchi, F. Hazama, I. Nagata, and H. Kataoka. Cerebral aneurysms arising at nonbranching sites. an experimental study. *Stroke*, 28(2):398–403, 1997.

[8] J. C. Lasheras. The biomechanics of arterial aneurysms. *Ann. Rev. Fluid Mech.*, 39:293–319, 2007.

[9] H. Mitsuoka, N. Unno, Y. Takei, T. Saito, K. Ishimaru, K. Miki, and S. Nakamura. Videodensitometric blood flow analysis of abdominal aortic aneurysm and intravascular coagulation. *J. Vasc. Surg.*, 38(2):340–345, 2003.

[10] L. Morris, P. Delassus, P. Grace, F. Wallis, M. Walsh, and T. McGloughlin. Effects of flat, parabolic and realistic steady flow inlet profiles on idealised and realistic stent graft fits through Abdominal Aortic Aneurysms (AAA). *Med. Eng. Phys.*, 28(1):19–26, 2006.

[11] M. L. Raghavan and D. A. Vorp. Toward a biomechanical tool to evaluate rupture potential of abdominal aortic aneurysm: Identification of a finite strain constitutive model and evaluation of its applicability. *J. Biomech.*, 33(4):475–482, 2000.

[12] M. L. Raghavan, D. A. Vorp, M. P. Federle, M. S. Makaroun, and M. W. Webster. Wall stress distribution on three-dimensionally reconstructed models of human abdominal aortic aneurysm. *J. Vasc. Surg.*, 31(4):760–769, 2000.

[13] G. J. Sheard, K. Hourigan, M. C. Thompson, and T. Leweke. Flow around an impulsively arrested circular cylinder. *Under consideration for publication in Phys. Fluids*, 2007.

[14] G. J. Sheard, T. Leweke, and K. Hourigan. The vortex trajectories invoked by an arresting cylinder. In P. J. Witt & P. Schwarz, editor, *Proceedings of the Fifth International Conference on CFD in the Process Industries*, Hilton on the Park, Melbourne, Australia, 2006. Published by CSIRO Australia. ISBN: 0-643-09423-7 CD-ROM.

[15] G. J. Sheard and K. Ryan. The flow past particles driven by a pressure gradient in small tubes. In P. J. Witt & P. Schwarz, editor, *Proceedings of the Fifth International Conference on CFD in the Process Industries*, Hilton on the Park, Melbourne, Australia, 2006. Published by CSIRO Australia. ISBN: 0-643-09423-7 CD-ROM.

[16] G. J. Sheard and K. Ryan. Pressure-driven flow past spheres moving in a narrow tube. *Under consideration for publication in J. Fluid Mech.*, 2007.

[17] D. A. Steinman, J. S. Milner, C. J. Norley S. P. Lownie, and D. W. Holdsworth. Image-based computational simulation of flow dynamics in a giant intracranial aneurysm. *J. Neuroradiol.*, 24(4):559–566, 2003.

[18] D. A. Steinman, D. A. Vorp, and C. R. Ethier. Computational modeling of arterial biomechanics: Insights into pathogenesis and treatment of vascular disease. *J. Vasc. Surg.*, 37(5):1118–1128, 2003.

[19] H. Ujiie, H. Tachibana, O. Hiramatsu, A. L. Hazel, T. Matsumoto, Y. Ogasawara, H. Nakajima, T. Hori, K. Takakura, and F. Kajiya. Effects of size and shape (aspect ratio) on the hemodynamics of saccular aneurysms: A possible index for surgical treatment of intracranial aneurysms. *Neurosurgery*, 45(1):119–129; discussion 129–130, 1999.